**Earthquakes and Structures**, *Vol. 18, No. 2* (*2020*) *147-162*
DOI: https://doi.org/10.12989/eas.2020.18.2.147


# Seismic performance assessments of precast energy dissipation shear wall structures under earthquake sequence excitations

Hao Zhang[1,3a], Chao Li*[2], Zhi-Fang Wang[1b] and Cai-Yan Zhang[2c]

[1]*School of Civil Engineering, Shenyang Jianzhu University, Shenyang 110168, China*
[2]*State Key Lab. of Coastal Offshore Engineering, Faculty of Infrastructure Engineering, Dalian University of Technology, Dalian 116024, China*
[3]*Guangdong Key Laboratory of Earthquake Engineering and Application Technology, Guangdong 510006, China*

(*Received September 4, 2019, Revised November 18, 2019, Accepted November 19, 2019*)

**Abstract.** This paper presents a novel precast energy dissipation shear wall (PEDSW) structure system that using mild steel dampers as dry connectors at the vertical joints to connect adjacent wall panels. Analytical studies are systematically conducted to investigate the seismic performance of the proposed PEDSW under sequence-type ground motions. During earthquake events, earthquake sequences have the potential to cause severe damage to structures and threaten life safety. To date, the damage probability of engineering structures under earthquake sequence has not been included in structural design codes. In this study, numerical simulations on single-story PEDSW are carried out to validate the feasibility and reliability of using mild steel dampers to connect the precast shear walls. The seismic responses of the PEDSW and cast-in-place shear wall (CIPSW) are comparatively studied based on nonlinear time-history analyses, and the effectiveness of the proposed high-rise PEDSW is demonstrated. Next, the foreshock-mainshock-aftershock type earthquake sequences are constructed, and the seismic response and fragility curves of the PEDSW under single mainshock and earthquake sequences are analyzed and compared. Finally, the fragility analysis of PEDSW structure under earthquake sequences is performed. The influences of scaling factor of the aftershocks (foreshocks) to the mainshocks on the fragility of the PEDSW structure under different damage states are investigated. The numerical results reveal that neglecting the effect of earthquake sequence can lead to underestimated seismic responses and fragilities, which may result in unsafe design schemes of PEDSW structures.

**Keywords:** PEDSW structure; seismic performance; earthquake sequence; fragility curve

## 1. Introduction

Precast structures have the advantages of a short construction period, resource conservation, and environmental protection, meeting the developmental needs of industrializing modern and green buildings (Park 2003, Nastri *et al.* 2017, Beilic *et al.* 2017). The shear wall has been widely used in precast structures due to its good integrity and high lateral resistance. However, the applied research and construction techniques of precast structures are still immature. Many problems exist in the design, construction, and quality control of shear wall connections in actual projects that directly affect the overall safety of the precast concrete shear wall (PCSW) structures (Magliulo *et al.* 2014). A large amount of seismic damage experience in the past has shown that the severe local damage caused by the insufficient strength of the connections between precast components can directly lead to brittle deformation or even collapse of the overall structure (Bljuger *et al.* 1976, Chakrabarti *et al.* 1988, Herfelt *et al.* 2016, Pall*et al.* 1982, Pekau *et al.* 1991, Pessiki *et al.* 2004, Zhang *et al. 2019*). Therefore, the proper seismic design of PCSW structures to ensure their seismic safety has become a research focus in the civil engineering fields.

There are a large number of horizontal and vertical connections in a PCSW structure, and the connections at the joints include two main types, namely, wet connections and dry connections (Fib-bulletin 43. 1999, Fib-bulletin 63. 2012). Wet connections are generally designed in the same manner as cast-in-place ones. Horizontal joints are generally connected by methods such as grouted lap-spliced or grouted sleeve connections, and vertical joints are usually connected in the form of the lap splicing of horizontal rebars reserved at the wall ends followed by concrete casting. Park (1995, 2002) reviewed the seismic design and construction methods of PCSWs used in New Zealand and detailed the common connection methods for horizontal and vertical joints. Chakrabarti *et al.* (1988) analyzed the test results of shear wall specimens and noted that the shear performance of the vertical joints is related to factors such as the strength of concrete at the connections and the number of rebars at the joints. Crisafulli *et al.* (2003) proposed a lightweight PCSW structural system that could be applied to low-rise buildings in high seismic regions, and discussed the seismic design theory of such wall panels. Lim *et al.* (2016) proposed T-shaped precast wall panels combining bolted connections and cast-in-place

*Corresponding author, Associate Professor
E-mail: chao.li@mail.dlut.edu.cn
[a]Associate Professor
E-mail: h_zhang@sjzu.edu.cn
[b]Postgraduate
[c]Ph.D. Candidate



ISSN: 2092-7614 (Print), 2092-7622 (Online)

concrete and verified their reliability and feasibility for engineering applications by cyclic loading tests. To evaluate the seismic performance of a single-row grouted sleeve connection, Xu *et al.* (2017) carried out static tests on a full-scale PCSW structure. The results showed that the failure mode, inter-story drift ratio (ISDR), ultimate load-carrying capacity, ductility, stiffness degradation, and energy dissipation of the precast structure are basically the same as those of the cast-in-place structure. Zhu *et al.* (2019) proposed a new type of PCSW with both grouted lap-spliced connection and cast-in-place concrete connection, and conducted a cyclic loading test on a 1⁄2 scaled four-story PCSW structural model. Their study showed that precast structural specimens have good integrity and complied with the seismic requirements of the Chinese seismic design code (GB50011, 2010).

The main types of dry connections for PCSWs include posttensioned connections, bolted connections, and welding. In recent years, a series of studies have been conducted on the dry connection technology and related seismic performance of PCSWs. Becker *et al.* (1980) conducted a nonlinear seismic response analysis of a posttensioned concrete shear wall and showed that shear slip occurred between the wall panels when the normal stress or friction coefficient of the horizontal joint was small. Rizkalla *et al.* (1989) carried out static tests on shear walls with horizontal joints, and they argued that horizontal shear keys can enhance the shear resistance of PCSW components. Soudki *et al.* (1995, 1996) further investigated the relationship between horizontal joints and the failure mode of wall panels. Based on an experimental analysis, Hutchinson *et al.* (1991) concluded that the load-carrying capacity of the horizontal joints and the shear capacity of the hollow floor slabs determine the shear performance of the horizontal joints of shear wall components. Kurama *et al.* (2005) connected the horizontal joints of a PCSW using a combination of mild steel and posttensioning bars. Pantelides *et al.* (2003) employed carbon fiber reinforced polymer (FRP) to strengthen the vertical joints of PCSWs. Srithara *et al.* (2015) proposed placing end columns on both sides of a PCSW panel and used energy-dissipating connectors to link the end columns with the wall panel to improve the energy dissipation capacity. Preze *et al.* (2007) placed ductile connectors at the vertical joints of an unbounded prestressed PCSW and investigated the seismic performance of the wall panel under a horizontal load. Guo *et al.* (2019) proposed a new method for the horizontal and vertical bolted connections of precast wall panels in low-rise PCSWs and conducted shaking table tests on a 1/2 scale PCSW structure to study the dynamic response characteristics and damage patterns of the structural model to validate the effectiveness of the proposed connection method. Under earthquakes, the vertical joints between the wall panels of a PCSW deform significantly. However, the conventional dry connections have poor energy dissipation capacity and are prone to damage. How to improve the energy dissipation capacity between the wall panels of a PCSW is essential to ensure the seismic safety of the structure.

In the above studies regarding the connection methods and seismic performance of PCSWs, the researchers generally only considered the impact of a single earthquake on the structural seismic performance. However, a large amount of historical seismic events have shown that the probability of only one mainshock occurring during an earthquake is extremely low, as the occurrence of a strong earthquake is often accompanied by multiple foreshocks and aftershocks. Previous studies (Jiang *et al.* 2006, Huang and Li. 2009) have shown that the earthquakes in the mainland of China can be divided into the mainshock-aftershock type, the earthquake sequence type, and the single mainshock type, which respectively account for 60%, 25%, and 15% of the total number of earthquakes. After the Mw 8.0 earthquake occurred in Wenchuan, China on May 12, 2008, a total of 54,971 aftershocks were recorded, with the largest reaching a magnitude of 6.4 (Huang and Li. 2009). On March 11, 2011, a Mw 8.6 earthquake occurred off the east coast of Honshu, Japan, followed by a total of 65 aftershocks with a magnitude of 6.0 or higher (Hirose *et al.* 2011). On August 8, 2017, a Mw 7.0 earthquake occurred in Jiuzhaigou, Sichuan, China, and a total of 1,334 aftershocks were recorded by the Sichuan Seismological Network, with the largest aftershock reaching a magnitude of 4.8 (Han *et al.* 2018). Engineering structures subjected to earthquakes may suffer from different levels of damage, and the foreshocks and aftershocks will inevitably exacerbate the degradation of the structural performance. Therefore, using earthquake sequences as inputs is beneficial for a more realistic assessment of the seismic performance of PCSW structures.

Mahin (1980) studied the response of a nonlinear single-degree-of-freedom (SDOF) system under real mainshock-aftershock sequence-type ground motions and noted that the aftershock may increase the ductility demand on the structure to a certain extent. Amadio *et al.* (2003) studied the elastoplastic response of a nonlinear SDOF system under earthquake sequence and pointed out that sequence-type ground motions may increase the cumulative damage of the structural system. Hatzigeorgiou *et al.* (2009, 2010) proposed a method for constructing mainshock-aftershock sequence-type ground motions based on the Gutenberg-Richter law, and reported that the mainshock-aftershock sequence-type ground motion increases the structural ductility demand compared with the single mainshock. The study by Liolios *et al.* (2014) showed that under a sequence-type ground motion, the displacement demand on structures increases and the resulting structural damage is severe; it was suggested that the effect of the mainshock-aftershock sequence must be considered in the seismic design of structures. As an important part of the performance-based seismic design of structures, the seismic fragility analysis predicts the conditional probability that a structure reaches or exceeds a certain ultimate failure state under different ground motion intensities and has been widely used in the seismic performance evaluation of engineering structures. Nazari *et al.* (2015) used an incremental dynamic analysis (IDA) method to study the seismic fragility of wood frame structures under mainshock-aftershock sequences. Li *et al.* (2014) constructed mainshock-aftershock sequences using three

(a) position of the joint (b) joint of T type (c) joint of L type

Fig. 1 Connected position and type of precast shear wall

methods (namely repetitive earthquake sequences, randomized earthquake sequences, and recorded earthquake sequences), and obtained the collapse probability of mainshock-damaged steel frame structures under aftershocks. Naderpour and Vakili (2019) assessed the seismic fragility of shear wall frame structures under mainshock-aftershock sequences. In summary, earthquake sequences could have a significant impact on the seismic damage and fragility of a structure. In the existing literature, however, there are very limited studies on the dynamic response and fragility of PCSW structures under earthquake sequences.

Recognizing the existing problems in the PCSW structures, a new type of precast energy-dissipation shear wall (PEDSW) structural system is presented by using mild steel dampers as dry connectors at the vertical joints of adjacent PCSWs. The seismic performance of the proposed PEDSW under earthquake sequences is investigated. Section 2 studies the quasi-static behavior of a single-layer PEDSW to validate the reliability of using mild steel dampers to connect the precast walls, the seismic performances of the PEDSW and cast-in-place shear wall (CIPSW) are comparatively studied based on nonlinear time-history analyses. In Section 3, the foreshock-mainshock-aftershock-type earthquake sequences are constructed and the dynamic responses of the PEDSW under single mainshock and earthquake sequences are analyzed and compared. Section 4 performs the fragility analysis of the PEDSW structure under earthquake sequences, and the influence of intensity ratio of the aftershock (foreshock) to the mainshock on the seismic fragility of the PEDSW structure was reported. Finally, the key concluding remarks of this paper is provided in Section 5.

## 2. Seismic performance of precast energy-dissipation shear wall (PEDSW)

Fig. 1 illustrates the method for the wet connection at the vertical joints of the wall panels in a typical PCSW. The reinforcing bars in the vertical joint area of the wall panel are very densely placed, making it difficult to place and vibrate concrete. As a result, it is difficult to guarantee the construction quality of the connections in the shear walls, thereby leading to a huge potential safety risk for the PCSW structures. In addition, the large amount of in situ wet operation required at the vertical joints of the PCSW also fundamentally limits the inherent advantages of the precast structure. Aiming at this problem, a new PEDSW using mild steel dampers as dry connectors at the vertical joints of adjacent precast walls is proposed in this paper. The embedded parts are reserved in the wall panels, and mild steel damper connectors are welded to the adjacent wall panels. On the one hand, this method avoids the need for horizontal rebar connections between the components of the PCSW (as shown in Figs. 1(b) and 1(c)) and limits the required amount of cast-in-place concrete, which is beneficial to the construction quality control. On the other hand, the input seismic energy can be dissipated by the mild steel dampers, thus reducing the seismic damage of the PCSW. In this section, based on numerical analyses, a quasi-static loading and a dynamic time-history analysis are conducted to compare the seismic performances of the PEDSW and the traditional CIPSW.

### *2.1 Static analysis of single-story PEDSW*

#### *2.1.1 Connector properties*

Mild steel dampers are low-cost and have a good energy-dissipation capacity and stable mechanical properties. Therefore, many researchers (Ozden and Ertas 2007, Sugata and Nakatsuka 2005, Sakata *et al.* 2005, Reaveley and Pantelides 2002) have systematically carried out theoretical and experimental investigations of the shape design and mechanical properties of mild steel dampers. The mild steel damper is a type of displacement-dependent damper. In the elastic stage, the mild steel damper relies on its stiffness to act as a connector, so no energy is dissipated. In the plastic phase, it can generate a large plastic deformation and thus dissipate seismic energy. In this study, a continuous round hole-type mild steel damper, as shown in Fig. 2 (a), was used to connect the wall panels of the PCSW. The damper had a hole radius of 55 mm and dimensions of 400 mm×500 mm. ABAQUS software (Simulia 2011) was used to simulate the mechanical properties of the damper under low-frequency cyclic loading. As shown in Figs. 2(b) and 2(c), the damper experienced a stress concentration in its main energy dissipation region (red area), had a full force-displacement

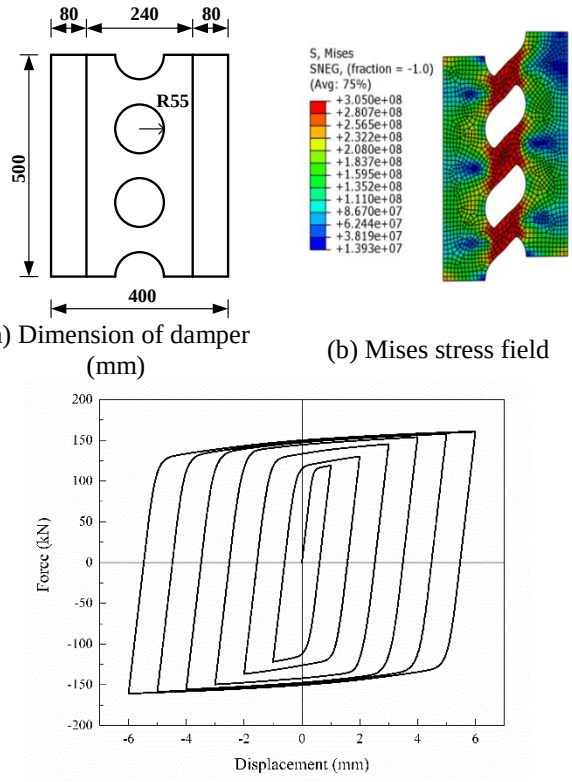


(a) Dimension of damper (mm)

(b) Mises stress field

(c) Load-displacement curve

Fig. 2 Schematic of the employed mild steel damper and its mechanical properties

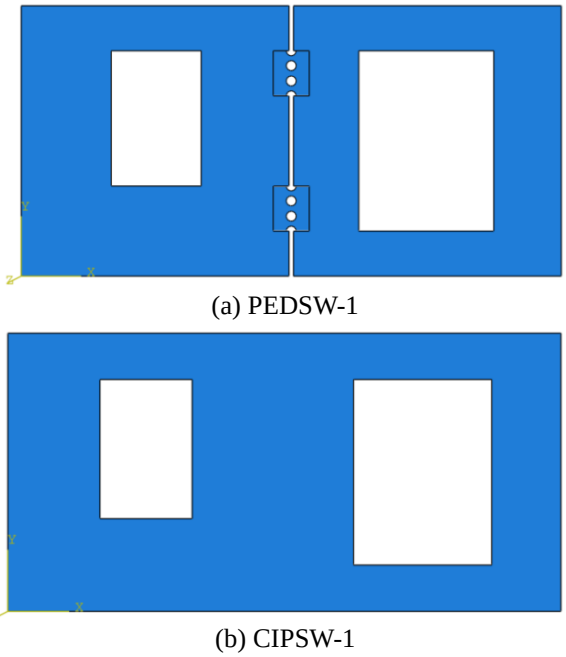

(a) PEDSW-1

(b) CIPSW-1

Fig. 3 FE models of PEDSW-1 and CIPSW-1

hysteresis curve, and exhibited an excellent energy dissipation capability.

### *2.1.2 Numerical model and analytical results*

To verify the reliability of using mild steel dampers as connectors at the vertical joints of the PCSW, the S4R element was used to simulate the single-story PEDSW (PEDSW-1), which was 3 m tall and 3 m wide. The left wall panel had an opening of 1 m×1.5 m, and the right wall panel had an opening of 1.5 m×2 m. Mild steel dampers, as shown in Fig. 2, were used to connect the wall panels on the two sides, and the wall panel reinforcement was designed using the rebar layer. The finite element (FE) model is shown in Fig. 3(a). Based on the same parameters, a corresponding FE model of a monolithic CIPSW (CIPSW-1) was established for comparative analysis, as shown in Fig. 3(b). The concrete damage plastic model and bilinear kinematic hardening model were used to model the concrete and rebar, respectively.

A vertical load and a monotonic horizontal displacement load were applied to the top of the wall. Fig. 4 shows the concrete Mises stress distribution of PEDSW-1 and CIPSW-1, which have similar Mises stresses and basically the same failure mode. Overall, the wall failed in shear, and the maximum stress occurred at the right-bottom of the wall. Fig. 5 compares the load-displacement curves of PEDSW-1 and CIPSW-1. The ultimate load-carrying capacities of

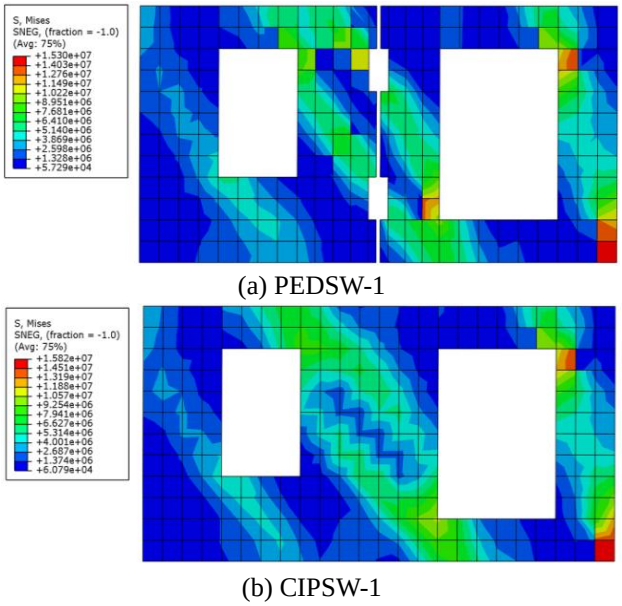


(a) PEDSW-1

(b) CIPSW-1

Fig. 4 Mises stress distribution of concrete for PEDSW-1 and CIPSW-1 (Pa)

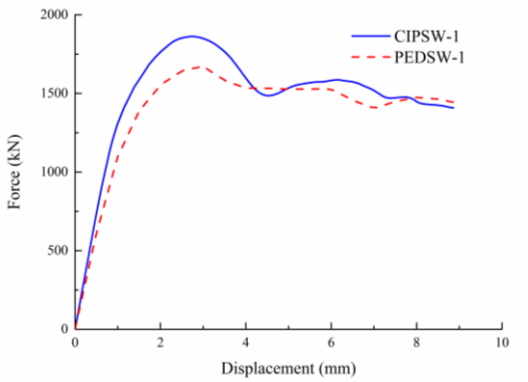


Fig. 5 Comparison of load-displacement curves of PEDSW-1 and CIPSW-1

CIPSW-1 and PEDSW-1 were 1860 kN and 1670 kN, respectively, with a difference of 11.38%. The PEDSW had basically the same load-carrying capacity and rigidity as the CIPSW. Therefore, it is feasible to use mild steel dampers as connectors at the vertical joints of precast concrete shear walls.

### *2.2 Nonlinear time history analysis of high-rise PEDSW*

#### *2.2.1 FE model of high-rise PEDSW*

The FE models of a high-rise PEDSW and a CIPSW were established to further verify the feasibility of applying the proposed mild steel dampers as connectors in the high-rise PCSW. A 16-story PCSW structure is used as the prototype. Fig. 6(a) shows three-dimensional and plan sketches of the prototype structure. The building has plan dimensions of 12 m×18 m. The adjacent upper and lower precast wall panels of the original structure are linked by sleeve grouted connections, and the vertical connection of the precast wall panels is in the form of lap splicing horizontal rebars and then pouring concrete.

Considering that the structure is symmetrical with an evenly distributed stiffness and the computational burden of the overall spatial structure is too large, to improve the analysis efficiency, a portion of shear walls in the prototype structure is selected to establish the FE model (PEDSW-2) of the high-rise PEDSW, with a story height of 3 m, a total height of 48 m, and a wall thickness of 0.2 m. The type of site for the location of prototype structure is the Class 2 site specified in the Chinese Seismic Design Code (GB50011, 2010). The wet connection at the joints of shear walls in the prototype structure was replaced with the mild steel dampers, as previously proposed in this paper. The setup and dimensions of the dampers were the same as those in the single-layer shear wall in Section 2.1. The FE model of the PEDSW-2 is shown in Fig. 6(c). Using the same parameters, the corresponding FE model of the CIPSW (CIPSW-2) was established, as shown in Fig. 6(d). Both the wall and dampers were modeled using the S4R element, which has good universality. The concrete strength of the wall was C30, a rebar layer was used to design the two-direction reinforcement, and the strength of the rebar was HRB400.

#### *2.2.2 Numerical results*

The modal analysis results showed that the periods of the first three modes of CIPSW-2 were 0.732s, 0.137s and 0.057s, respectively, while the periods of the first three modes of PEDSW-2 were 0.738s, 0.138s and 0.058s, respectively. Because the use of mild steel dampers to assemble the precast wall panels weakened the stiffness of the shear wall structure to some extent, the structural period of PEDSW-2 was slightly larger than that of CIPSW-2. From the PEER Strong Ground Motion Database, 20 real ground motions with a wide range of magnitudes and epicentral distances were selected as seismic inputs to conduct nonlinear time-history analyses of PEDSW-2 and CIPSW-2. The results of the time-history analysis were extracted, and the maximum roof displacement and ISDR were used as structural response indicators. Table 1 lists the maximum roof displacements and ISDRs, as well as the corresponding reduction percentages (RPs) of PEDSW-2 and CIPSW-2 under various earthquake excitations. The results showed that the overall structural responses of PEDSW-2 were smaller than that of CIPSW-2, with the maximum roof displacement reduced by 7.91% to 45.15% and the maximum ISDR reduced by 7.61% to 44.53%.

Fig. 7 and Fig. 8 compare the roof displacement time histories and ISDRs of PEDSW-2 and CIPSW-2 under GO3-090 and CAP-000 ground motions, respectively. The maximum roof displacement and ISDR of PEDSW-2 are smaller than those of CIPSW-2. As the story increases, the ISDR of PEDSW-2 exhibits a significant decreasing trend compared to that of CIPSW-2. The maximum ISDRs of PEDSW-2 under GO3-090 and CAP-000 are $3.50\times10^{-3}$ and $4.48\times10^{-3}$, respectively, amounting to reductions of 22.74% and 18.69%, respectively, compared with those of CIPSW-2. Fig. 9 compares the concrete compression damage of walls under GO3-090 and CAP-000. It can be seen from the contour plot of the compression damage that the damage level of PEDSW-2 was significantly reduced. Compared to CIPSW-2, the maximum compression damage extents of PEDSW-2 decrease by 10.66% and 13.38%, respectively.

Based on the above analysis, it can be concluded that, as a precast wall connector, the mild steel damper is able to not only effectively connect the shear walls but also reduce the structural seismic responses. In addition, the mild steel damper can effectively reduce the concrete damage of the shear wall panels. Therefore, the proposed PEDSW, in which mild steel dampers are used as dry connectors at the vertical joints of the PCSW, is both feasible and effective as a new structural system.

## 3. Structural seismic response analysis under earthquake sequences

### *3.1 Construction of earthquake sequences*

Depending on whether foreshocks are presented, the earthquake sequence can be divided into two types, namely the foreshock-mainshock-aftershock type and the mainshock-aftershock type. Because of the small number of actually recorded earthquake sequence-type ground motions, researchers have used different methods for constructing sequence-type ground motions to study their destructive effect on building structures. Li and Ellingwood (2007) gave the magnitude of mainshocks according to probability density functions of the magnitudes of the aftershocks and obtained the probability distribution of the maximum magnitude of the aftershocks through Monte Carlo simulation. Wen (2017) used a ground motion attenuation formula to determine and scale the amplitude of the peak ground acceleration (PGA) value according to the fault distance and randomly combined different single ground motions to construct mainshock-aftershock sequence-type ground motions. Based on the Gutenberg-Richter law and the Joyner-Boore attenuation relation, Hatzigeorgiou *et al.* (2009, 2010) proposed a method to

Table 1 Comparison of maximum top displacement and ISDR between PEDSW-2 and CIPSW-2

| No. | Earthquake motion | PGA(g) | Top displacement (mm) | | | ISDR ($10^{-3}$) | | |
|---|---|---|---|---|---|---|---|---|
| | | | CIPSW-2 | PEDSW-2 | RP(%) | CIPSW-2 | PEDSW-2 | RP(%) |
| 1 | M-AGW-140 | 0.032 | 36.23 | 29.12 | 19.62 | 1.03 | 0.81 | 21.36 |
| 2 | H06-360 | 0.06 | 26.12 | 21.71 | 16.88 | 0.77 | 0.61 | 20.78 |
| 3 | A-HAR-090 | 0.07 | 72.1 | 54.31 | 24.67 | 1.97 | 1.47 | 25.38 |
| 4 | LOA-092 | 0.086 | 86.04 | 65.19 | 24.23 | 2.27 | 1.77 | 22.03 |
| 5 | BRA-315 | 0.16 | 46.02 | 32.61 | 29.14 | 1.47 | 1.07 | 27.21 |
| 6 | DWN-360 | 0.23 | 82.23 | 59.41 | 27.75 | 2.07 | 1.61 | 22.22 |
| 7 | CO8-320 | 0.259 | 69.93 | 56.82 | 18.75 | 1.91 | 1.54 | 19.37 |
| 8 | SLC-360 | 0.277 | 113.45 | 93.05 | 17.98 | 3.01 | 2.44 | 18.94 |
| 9 | M-HVR-240 | 0.302 | 160.21 | 142.81 | 10.86 | 4.47 | 3.64 | 18.57 |
| 10 | CEN-245 | 0.321 | 126.57 | 98.39 | 22.26 | 3.33 | 2.6 | 21.92 |
| 11 | H-AEP-045 | 0.334 | 123.52 | 103.79 | 15.97 | 4.01 | 3.21 | 19.95 |
| 12 | GO3-090 | 0.364 | 145.45 | 126.86 | 12.78 | 4.53 | 3.5 | 22.74 |
| 13 | LOS-000 | 0.411 | 218.37 | 167.32 | 23.38 | 6.51 | 4.37 | 32.87 |
| 14 | GO4-000 | 0.413 | 198.36 | 108.81 | 45.15 | 5.03 | 2.79 | 44.53 |
| 15 | CAP-000 | 0.511 | 191.26 | 172.25 | 9.94 | 5.51 | 4.48 | 18.69 |
| 16 | H-BCR-140 | 0.59 | 224.15 | 163.43 | 27.09 | 6.33 | 5.23 | 17.38 |
| 17 | NWH-360 | 0.59 | 414.43 | 348.59 | 15.89 | 10.67 | 8.28 | 22.4 |
| 18 | SYL--090 | 0.604 | 354.73 | 326.67 | 7.91 | 9.33 | 8.31 | 10.93 |
| 19 | H-BCR-230 | 0.78 | 396.29 | 307.56 | 22.39 | 8.67 | 8.01 | 7.61 |
| 20 | SPV-360 | 0.939 | 327.15 | 267.59 | 18.21 | 9.67 | 8.88 | 8.17 |

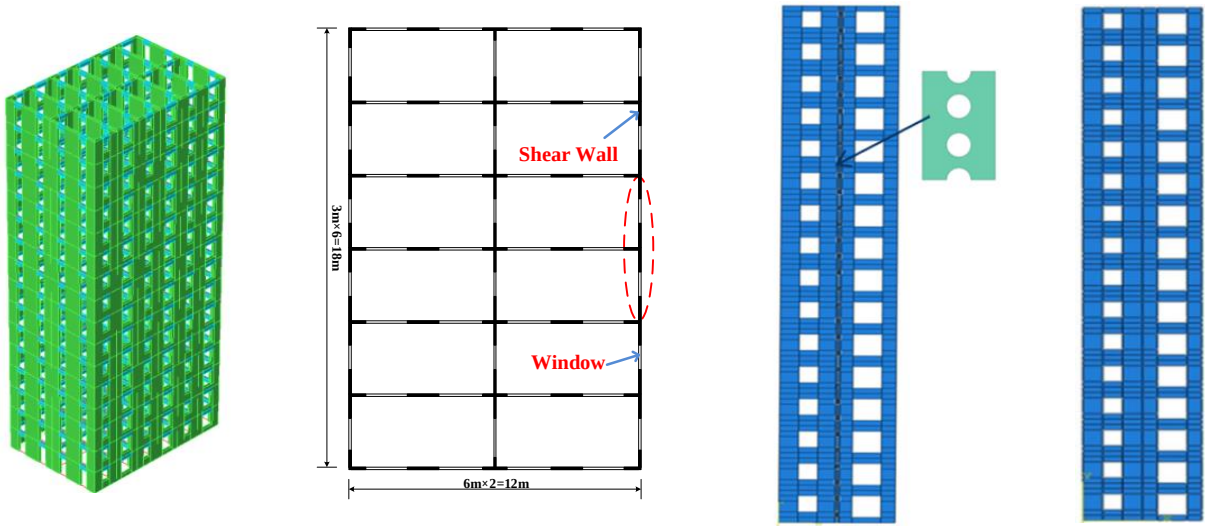


(a) Structural layout (b) Plan view (c) PEDSW-2 (d) CIPSW-2

Fig. 6 Exemplar precast shear wall structure and the corresponding FE models of PEDSW-2 and CIPSW-2

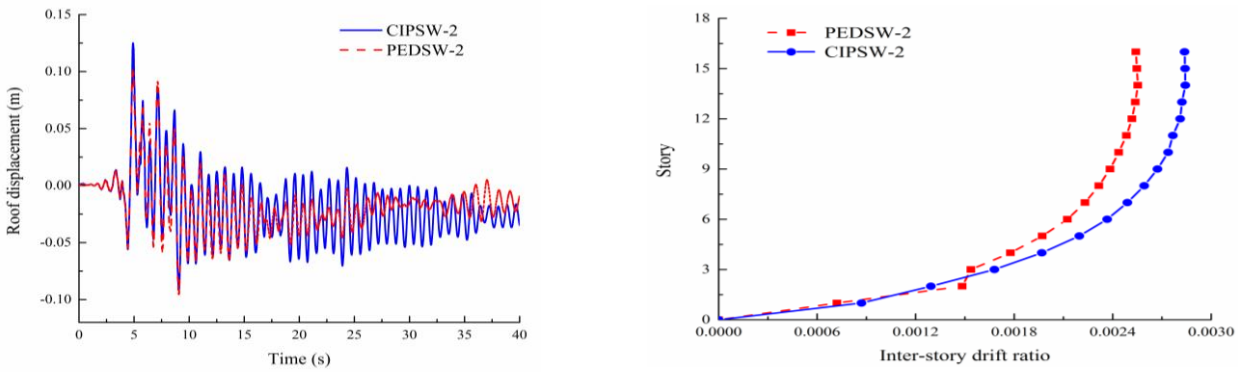


(a) Roof displacement time histories (b) ISDRs

Fig. 7 Seismic responses of PEDSW-2 and CIPSW-2 under earthquake GO3-090 (PGA=0.364g)

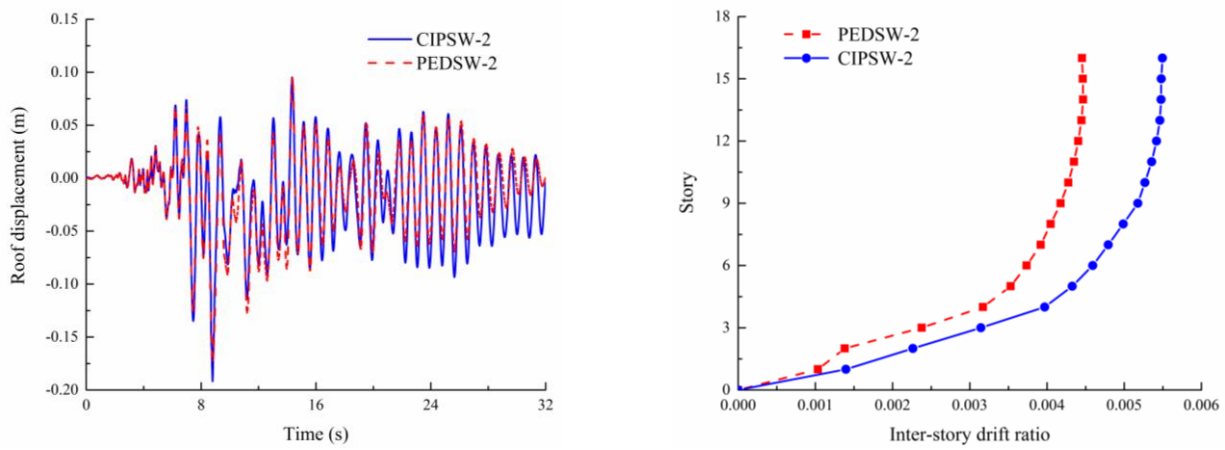


(a) Roof displacement time histories (b) ISDRs

Fig. 8 Seismic responses of PEDSW-2 and CIPSW-2 under earthquake CAP-000 (PGA=0.511g)

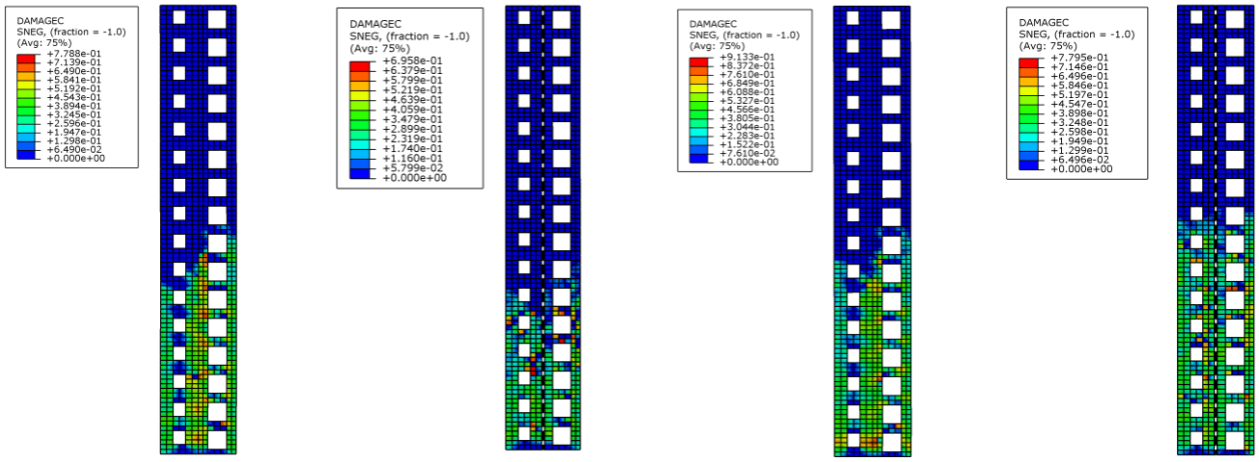


(a) CIPSW-2(GO3-090) (b) PEDSW-2(GO3-090) (c) CIPSW-2(CAP-000) (d) PEDSW-2(CAP-000)

Fig. 9 Comparison between concrete compression damage of PEDSW-2 and CIPSW-2

obtain a foreshock-mainshock-aftershock sequence by continuously repeating one ground motion three times and scaling the PGAs with factors of 0.8526, 1.0 and 0.8526, respectively. However, the derivation of the scaling factor ($\delta$) for the PGA did not use specific seismic record information, and the proposed scaling factor ($\delta$=0.8526) may overestimate the intensity of the foreshock and aftershock, thus posing a certain limitation.

In this study, a foreshock-mainshock-aftershock sequence is constructed based on the method proposed by Hatzigeorgiou *et al.* (2009, 2010). Taking into account the uncertainty of the ratios of the PGAs of the foreshock and aftershock to that of mainshock, the scaling factor $\delta$ was set to 0.4, 0.6 and 0.8, to study its effect on the seismic response of the PEDSW. First, the ground motion records were selected, and the acceleration time histories were multiplied by $\delta$ to obtain the foreshock and aftershock. Then, the time interval between the foreshock and mainshock, as well as between the mainshock and aftershock, was set as 50*s* to ensure that the structure returns to the stationary state before it is subjected to the following ground motions. Finally, the ground motion acceleration time histories and the interval segments are spliced together to obtain the foreshock-mainshock-aftershock sequences, thus taking into account the effect of the earthquake sequence on the cumulative damage of structures.

### *3.2 Numerical results*

According to the aforementioned method, the foreshock-mainshock-aftershock sequences were constructed with different $\delta$ values using the 20 recorded ground motions selected in Section 2.2.2. Here, a total of 80 sets of ground motions, including 20 sets of single mainshocks and 20 sets of earthquake sequences, each with $\delta$ being 0.4, 0.6, and 0.8, were used as inputs in the nonlinear time-history analyses. The PEDSW (i.e., PEDSW-2) in Section 2.2.2 was used as an example to study the effect of the earthquake sequence on the structural seismic response.

#### *3.2.1 Maximum roof displacements*

Table 2 lists the maximum roof displacements of PEDSW-2 under single mainshocks and earthquake sequences, as well as the increase ratio (IR) of roof displacement under earthquake sequences. According to

Table 2 Comparison of maximum top displacement of PEDSW-2 under mainshock and earthquake sequences (mm)

| No. | Earthquake motion | PGA($g$) | Mainshocks | Earthquake sequences | | | | | |
|---|---|---|---|---|---|---|---|---|---|
| | | | | $\delta$=0.4 | IR (%) | $\delta$=0.6 | IR (%) | $\delta$=0.8 | IR (%) |
| 1 | M-AGW-140 | 0.032 | 29.12 | 34.83 | 19.61 | 36.52 | 25.41 | 37.56 | 28.98 |
| 2 | H06-360 | 0.06 | 21.71 | 26.33 | 21.28 | 33.28 | 53.29 | 33.29 | 53.34 |
| 3 | A-HAR-090 | 0.07 | 54.31 | 79.32 | 46.05 | 82.28 | 51.5 | 88.11 | 62.24 |
| 4 | LOA-092 | 0.086 | 65.19 | 65.96 | 1.18 | 66.83 | 2.52 | 70.68 | 8.42 |
| 5 | BRA-315 | 0.16 | 32.61 | 33.76 | 3.53 | 33.82 | 3.71 | 34.51 | 5.83 |
| 6 | DWN-360 | 0.23 | 59.41 | 67.88 | 14.26 | 66.49 | 11.92 | 68.54 | 15.37 |
| 7 | CO8-320 | 0.259 | 56.82 | 59.72 | 5.1 | 60.64 | 6.72 | 61.04 | 7.43 |
| 8 | SLC-360 | 0.277 | 93.05 | 138.12 | 48.44 | 150.54 | 61.78 | 160.23 | 72.2 |
| 9 | M-HVR-240 | 0.302 | 142.81 | 152.68 | 6.91 | 159.38 | 11.6 | 168.97 | 18.32 |
| 10 | CEN-245 | 0.321 | 98.39 | 134.21 | 36.41 | 137.26 | 39.51 | 178.36 | 81.28 |
| 11 | H-AEP-045 | 0.334 | 103.79 | 118.39 | 14.07 | 120.33 | 15.94 | 150.01 | 44.53 |
| 12 | GO3-090 | 0.364 | 126.86 | 139.27 | 9.78 | 147.4 | 16.19 | 145.27 | 14.51 |
| 13 | LOS-000 | 0.411 | 167.32 | 176.39 | 5.42 | 186.32 | 11.36 | 203.81 | 21.81 |
| 14 | GO4-000 | 0.413 | 108.81 | 115.28 | 5.95 | 117.93 | 8.38 | 140.31 | 28.95 |
| 15 | CAP-000 | 0.511 | 172.25 | 236.86 | 37.51 | 254.71 | 47.87 | 232.61 | 35.04 |
| 16 | H-BCR-140 | 0.59 | 163.43 | 287.17 | 75.71 | 291.23 | 78.2 | 289.23 | 76.97 |
| 17 | NWH-360 | 0.59 | 348.59 | 357.65 | 2.6 | 425.75 | 22.13 | 497.56 | 42.74 |
| 18 | SYL--090 | 0.604 | 326.67 | 580.29 | 77.64 | 582.12 | 78.2 | 588.55 | 80.17 |
| 19 | H-BCR-230 | 0.78 | 307.56 | 328.78 | 6.9 | 383.65 | 24.74 | 456.32 | 48.37 |
| 20 | SPV-360 | 0.939 | 267.59 | 354.68 | 32.55 | 426.39 | 59.34 | 493.31 | 84.35 |

Table 2, when $\delta$=0.4, the IR of the maximum roof displacement is in the range of 1.18% to 77.64%; when $\delta$=0.6, the IR of the maximum roof displacement is in the range of 2.52% to 78.2%; and when $\delta$=0.8, the IR of the maximum roof displacement is in the range of 5.83% to 84.35%. Compared to that under single mainshocks, the maximum roof displacement of PEDSW-2 under earthquake sequences increases to different extents, and the IR of the maximum roof displacement of PEDSW-2 also shows an increasing trend as the scaling factor $\delta$ increases. Fig. 10 compares the roof displacement time histories of PEDSW-2 under a single mainshock and the corresponding earthquake sequences of the GO-4000 ground motion. As shown, the maximum roof displacement of the structure under earthquake sequences exhibits an increasing trend. When the scaling factor of the earthquake sequence is $\delta$=0.4, the maximum roof displacement of PEDSW-2 increases by 5.95%, while the IR of the response reaches 28.95% when $\delta$=0.8.

### 3.2.2 Maximum ISDRs

Table 3 lists the maximum ISDRs of PEDSW-2 under single mainshocks and earthquake sequences ($\delta$=0.4, 0.6, 0.8). According to the table, when $\delta$=0.4, the IR of the maximum ISDR is in the range of 1.69% to 60.8%; when $\delta$=0.6, the IR of the ISDR is in the range of 2.49% to 72.32%; and when $\delta$=0.8, the IR of the ISDR is in the range of 11.04% to 81.83%. Compared with that under a single mainshock, the maximum ISDR of PEDSW-2 under earthquake sequences increases to different extents, and as the scaling factor $\delta$ increases, the IR of the ISDR of PEDSW-2 shows an overall increasing trend. It should be noted that under H-BCR-140, the maximum ISDR of the PEDSW-2 is $5.23\times10^{-3}$, which meets the requirement of ISDR<1/120 from the Chinese seismic design code (GB50011, 2010). In comparison, the maximum ISDRs under the earthquake sequences ($\delta$=0.4, 0.6, 0.8) are $8.41\times10^{-3}$, $8.94\times10^{-3}$ and $8.82\times10^{-3}$, all exceeding the allowable value of the Code (GB50011, 2010). Fig. 11(a) shows the envelope curves of the ISDRs of PEDSW-2 under a single mainshock (GO4-000) and the earthquake sequences ($\delta$=0.4, 0.6, 0.8). The ISDR curve under the first earthquake sequence ($\delta$=0.4) is similar to that under a single mainshock. As the story increases, the ISDR curve under the third earthquake sequence ($\delta$=0.8) exhibits the most significant increasing trend.

Figs. 11(a), 11(b), and 11(c) compare the maximum ISDRs of PEDSW-2 under a single mainshock and those under earthquake sequences ($\delta$=0.4, 0.6, 0.8). When the scaling factor of the earthquake sequence is $\delta$=0.4, the IR of the maximum ISDR of PEDSW-2 is 3.58%; while the corresponding IR reaches 33.33% when $\delta$=0.8.

### 3.2.3 Concrete damage of shear walls

For the high-rise PCSW structures, the wall bottom is where the most severe damage occurs. The concrete damage factor can be output by the ABAQUS platform. Fig. 12 compares the compression damage of PEDSW-2 under a single mainshock and different earthquake sequences ($\delta$=0.4, 0.6, 0.8) of the CO8-320 ground motion. Compared with that under a single mainshock, the concrete compression damage of the wall under the earthquake sequences is more severe, indicating that the foreshock-mainshock-aftershock-type earthquake sequence can exacerbate the concrete compression damage to some extent. Under a single mainshock, the maximum concrete compression damage factor is 0.765; under the earthquake sequence with $\delta$=0.4, the concrete compression damage

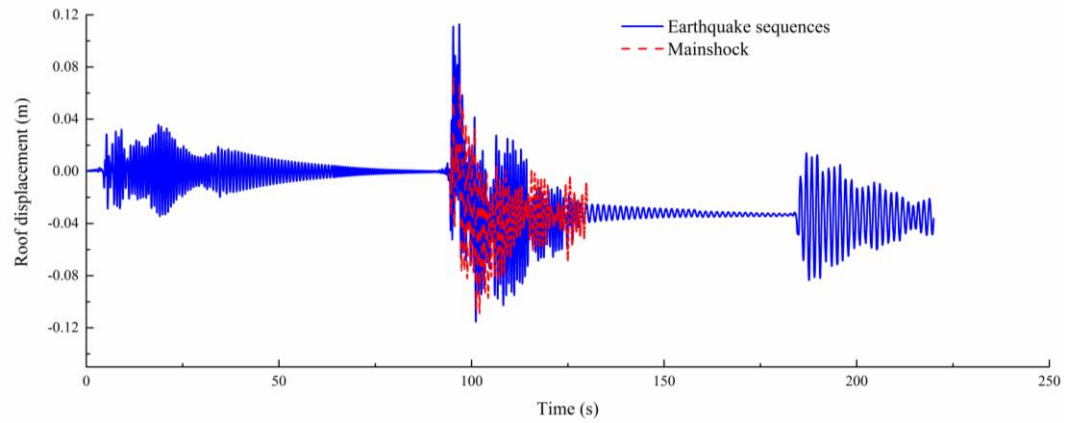


(a) $\delta$=0.4

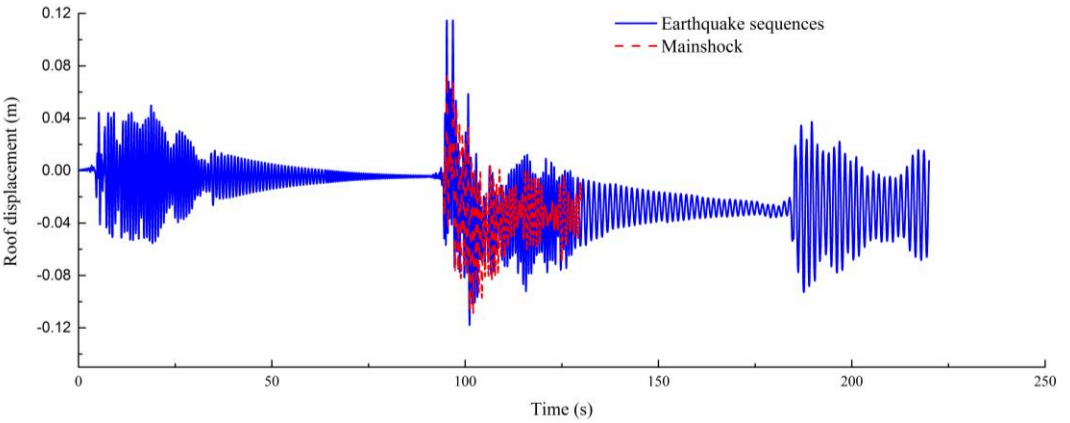


(b) $\delta$=0.6

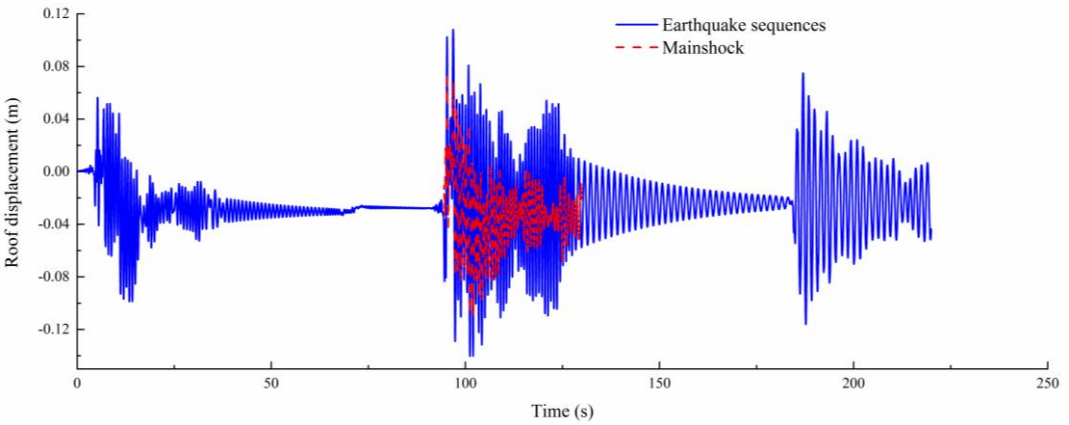


(c) $\delta$=0.8

Fig. 10 Comparison of top displacement time-histories under mainshock and earthquake sequences (GO4000, PGA = 0.413g)

factor is 0.778, amounting to an increase of 1.70% compared to that under the single mainshock; when $\delta$=0.6, the concrete compression damage factor is 0.804, representing an increase of 5.10% over that under the single mainshock; and when $\delta$=0.8, the concrete compression damage factor is 0.821, which is 7.32% higher than that under the single mainshock. Therefore, the concrete compression damage under earthquake sequences shows an increasing trend with the increase of the δ value.

It can be seen from the above analysis that the foreshock-mainshock-aftershock-type earthquake sequence can cause additional damage, exacerbate the performance degradation, and increase the roof displacement, ISDR, and concrete damage, thus adversely affecting the PEDSW structure. In addition, the effects of the foreshock and aftershock on the structural seismic response increase with the intensity. Therefore, the use of a single mainshock in traditional seismic analysis methods to calculate the structural seismic response would overestimate the seismic performance of a structure to some extent, thus it is of great practical significance to study the responses of new structural systems such as the PEDSW under earthquake sequences.

Table 3 Comparison of maximum top displacement of PEDSW-2 under mainshocks and earthquake sequences (mm)

| No. | Earthquake motion | PGA(g) | Mainshocks | Earthquake sequences | | | | | |
|---|---|---|---|---|---|---|---|---|---|
| | | | | $\delta$=0.4 | IR (%) | $\delta$=0.6 | IR (%) | $\delta$=0.8 | IR (%) |
| 1 | M-AGW-140 | 0.032 | 0.81 | 0.84 | 3.7 | 0.93 | 14.81 | 1.03 | 27.16 |
| 2 | H06-360 | 0.06 | 0.61 | 0.65 | 6.56 | 0.8 | 31.15 | 0.87 | 42.62 |
| 3 | A-HAR-090 | 0.07 | 1.47 | 2.06 | 40.14 | 2.13 | 44.9 | 2.12 | 44.22 |
| 4 | LOA-092 | 0.086 | 1.77 | 1.88 | 6.21 | 1.96 | 10.73 | 2.07 | 16.95 |
| 5 | BRA-315 | 0.16 | 1.07 | 1.13 | 5.61 | 1.18 | 10.28 | 1.21 | 13.08 |
| 6 | DWN-360 | 0.23 | 1.61 | 1.78 | 10.56 | 1.76 | 9.32 | 1.8 | 11.8 |
| 7 | CO8-320 | 0.259 | 1.54 | 1.62 | 5.19 | 1.68 | 9.09 | 1.71 | 11.04 |
| 8 | SLC-360 | 0.277 | 2.44 | 2.93 | 20.08 | 3.41 | 39.75 | 4.13 | 69.26 |
| 9 | M-HVR-240 | 0.302 | 3.64 | 3.79 | 4.12 | 4.12 | 13.19 | 4.3 | 18.13 |
| 10 | CEN-245 | 0.321 | 2.6 | 3.4 | 30.77 | 3.94 | 51.54 | 4.2 | 61.54 |
| 11 | H-AEP-045 | 0.334 | 3.21 | 3.33 | 3.74 | 3.29 | 2.49 | 4.09 | 27.41 |
| 12 | GO3-090 | 0.364 | 3.5 | 3.7 | 5.71 | 4.52 | 29.14 | 4.16 | 18.86 |
| 13 | LOS-000 | 0.411 | 4.37 | 4.93 | 12.81 | 5.07 | 16.02 | 5.33 | 21.97 |
| 14 | GO4-000 | 0.413 | 2.79 | 2.89 | 3.58 | 3.01 | 7.89 | 3.72 | 33.33 |
| 15 | CAP-000 | 0.511 | 4.48 | 5.79 | 29.24 | 5.97 | 33.26 | 6.42 | 43.3 |
| 16 | H-BCR-140 | 0.59 | 5.23 | 8.41 | 60.8 | 8.94 | 70.94 | 8.82 | 68.64 |
| 17 | NWH-360 | 0.59 | 8.28 | 8.42 | 1.69 | 9.68 | 16.91 | 11.97 | 44.57 |
| 18 | SYL-090 | 0.604 | 8.31 | 13.02 | 56.68 | 14.32 | 72.32 | 15.11 | 81.83 |
| 19 | H-BCR-230 | 0.78 | 8.01 | 8.29 | 3.5 | 8.63 | 7.74 | 9.92 | 23.85 |
| 20 | SPV-360 | 0.939 | 8.88 | 11.78 | 32.66 | 13.52 | 52.25 | 15.23 | 71.51 |

## 4. Fragility analysis of PEDSW under earthquake sequences

With the development of civil engineering technology, engineers and academic researchers have gradually realized that merely increasing the structural strength does not necessarily guarantee the structural safety. Therefore, performance-based seismic design (PBSD) has received increasing attention (Fajfar 2000, Li *et al.* 2015, Allahvirdizadeh and Mohammadi. 2016, Li *et al.* 2017, Li *et al.* 2017, Zhang *et al.* 2018). Structural fragility analysis has become an important component of PBSD, and structural fragility has become a research focus in the civil engineering field (Li *et al.* 2016, 2018, Li *et al.* 2018, Li *et al.* 2018). The seismic fragility is the probability that a structure reaches a certain damage state under earthquakes of different intensities. It quantitatively characterizes the seismic performance of an engineering structure from the perspective of probability and describes the relationship between the structural damage degree and the ground motion intensity from a macroscopic point of view. Here, using the high-rise PEDSW (PEDSW-2) as the research object and the foreshock-mainshock-aftershock sequences as the ground motion inputs, the seismic fragility of the PEDSW structure was calculated based on the probabilistic seismic demand analysis (PSDA) method.

### *4.1 Probabilistic seismic demand model under earthquake sequences*

The probabilistic seismic demand model (PSDM) characterizes the relationship between the engineering demand parameter (EDP) and the ground motion intensity measure (IM) based on the dynamic nonlinear time-history analysis results of a structure. Commonly used approaches include the cloud approach and the scaling approach. In particular, the scaling approach uses different ratios to scale the selected ground motions to different intensities and then uses the scaled ground motions as inputs for the structural model to obtain the structural responses. This approach requires a large amount of scaling calculation, and hence its operation efficiency is low. In this paper, the cloud approach is adopted to calculate the PSDM of PEDSW-2. Cornell *et al.* (2002) reported that the EDP and the ground motion IM have a logarithmic linear relationship

$$\ln(EDP) = \ln a + b\ln(IM) \tag{1}$$

where $a$ and $b$ are logarithmic linear regression parameters. The logarithmic linear fitting of the seismic responses of PEDSW-2 gives the PSDM. The standard deviation is expressed as:

$$\sigma_{D|IM} = \sqrt{\frac{\sum_{i=1}^{N}\left[\ln(D_i) - \ln(aIM_i^{\,b})\right]^2}{N-2}} \tag{2}$$

where $N$ is the number of samples in the regression analysis, $N$ = 80 in this study; $D_i$ is the peak value of the $i$th seismic demand; and $IM_i$ is the peak value of the $i$th ground motion. The smaller the logarithmic standard deviation is, the better goodness of fit of the regression is.

The ground motion uncertainty and structural uncertainty are the two main uncertainty factors in a fragility analysis. Kwon and Elnashai (2006) carried out a shaking table test and numerical simulation on a three-story

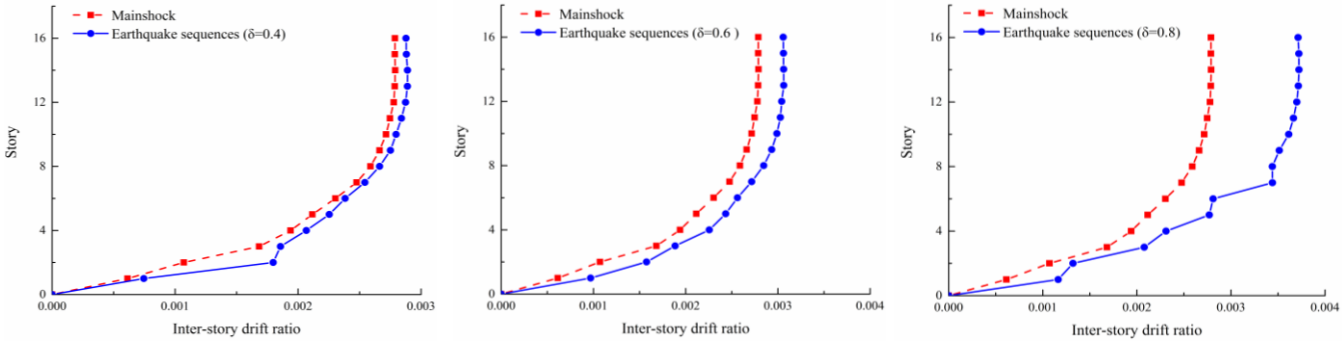


(a) $\delta$=0.4 (b) $\delta$=0.6 (c) $\delta$=0.8

Fig. 11 Comparison of ISDRs under mainshocks and earthquake sequences (GO4-000, PGA=0.413 g)

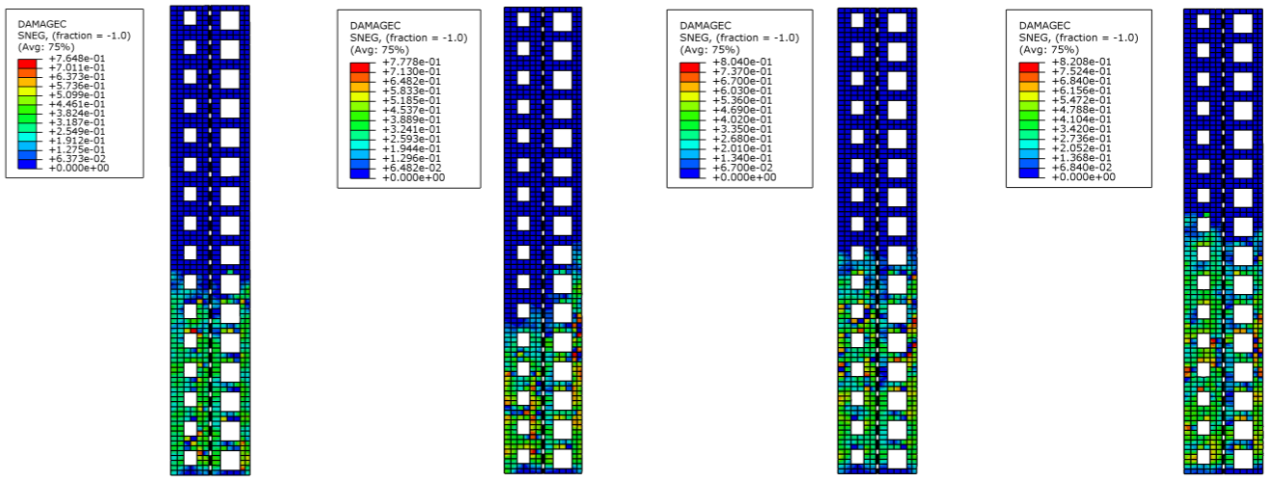


(a) Mainshock (b) Sequence ($\delta$=0.4) (c) Sequence ($\delta$=0.6) (d) Sequence ($\delta$=0.8)

Fig. 12 Comparison of concrete compression damage of PEDSW-2 under mainshocks and earthquake sequences (CO8-320, PGA = 0.259 g)

RC frame structure to study the effects of uncertainties in strong earthquake ground motion and structural parameters on the structural fragility. The results of their study indicated that the ground motion uncertainty has a more severe effect on the fragility analysis, far greater than the effect of structural uncertainty. In addition, in many previous studies on the structural seismic fragility, some researchers have confirmed that the structural parameter uncertainty has a very small influence on the PSDM compared with the ground motion uncertainty (e.g., Shrestha *et al.* 2017). Therefore, only the effect of the ground motion uncertainty is considered herein.

The ground motion itself is highly random, as it is affected by a number of factors such as the magnitude, epicentral distance, and seismic wave propagation path. In this study, the ground motions were selected over a wide range of magnitudes and epicentral distances using the bin approach (Shome and Cornell 1999). The following five ground motion bins defined by Mackie and Stojadinović (2005) are employed: small magnitude and small distance (SMSR, 5.8<$M_w$<6.5, 13<$R$<30 km), large magnitude and small distance (LMSR, 6.5<$M_w$<7.0, 13<$R$<30 km), small magnitude and large distance (SMLR, 5.8<$M_w$<6.5, 30<$R$<60 km), large magnitude and large distance (LMLR, 6.5<$M_w$<7.0, 30<$R$<60 km), and near-fault ground motions

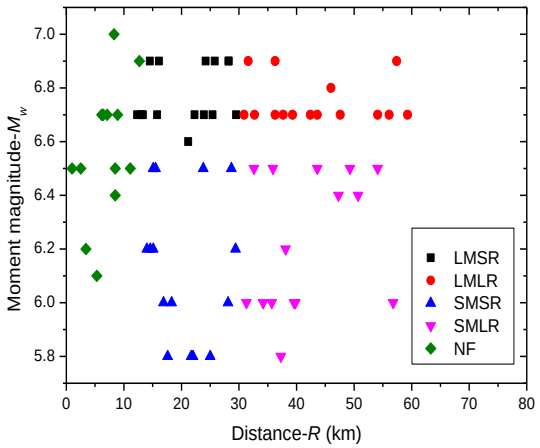


Fig. 13 Selected ground motion records in Mw-R space

(NF,R<13 km). A total of 75 ground motions (15 in each of the 5 bins) were selected from the PEER Strong Ground Motion Database to comprehensively consider the effect of ground motion randomness on the calculation accuracy of the numerical simulation. The distribution of the $M_w$-$R$ of the selected ground motion records is shown in Fig. 13. According to the earthquake sequence construction method described in Section 3.2, the75 selected seismic records

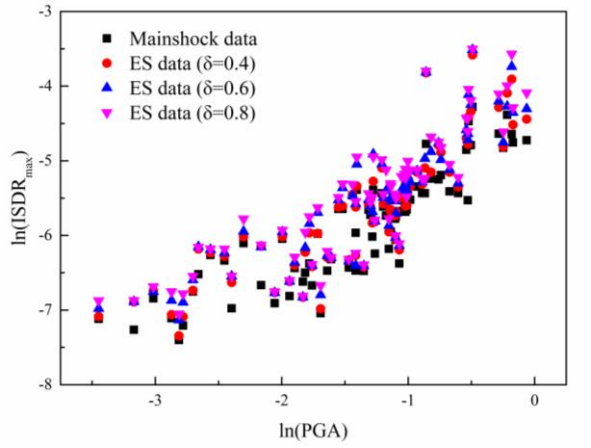


(a) EDP values for all cases

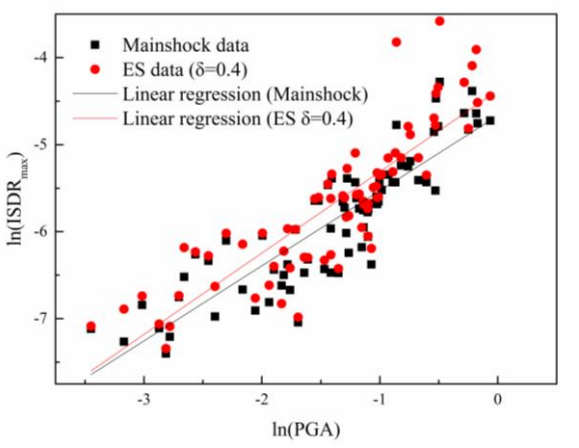


(b) Mainshock and earthquake sequence ($\delta$=0.4)

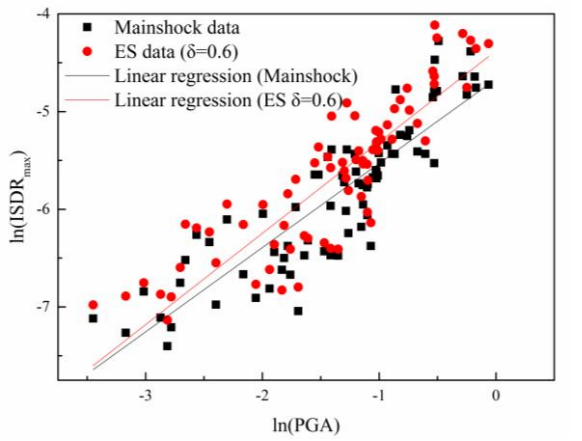


(c) Mainshock and earthquake sequence ($\delta$=0.6)

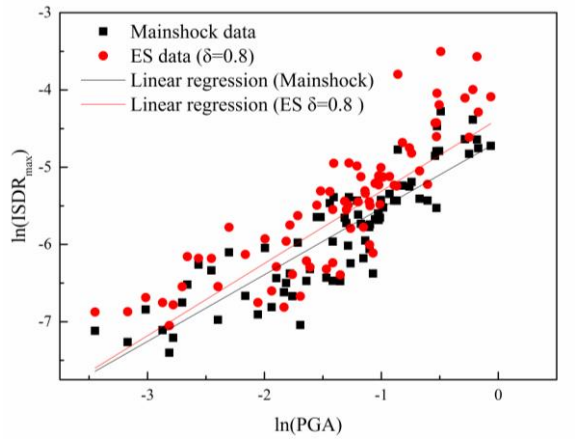


(d) Mainshock and earthquake sequence ($\delta$=0.8)

Fig. 14 Regression analysis of EDP and IM under mainshock and earthquake sequences

Table 4 Parameters for the probabilistic demand models

| Cases | Regression model | $R^2$ | $\sigma_{D\|IM}$ |
|---|---|---|---|
| Mainshock | $\ln(ISDR_{max})$ = -4.667+0.86255ln ($PGA$) | 0.769 | 0.1335 |
| Earthquake sequence$\delta$ = 0.4 | $\ln(ISDR_{max})$ = -4.376+0.93489ln ($PGA$) | 0.741 | 0.1830 |
| Earthquake sequence$\delta$ = 0.6 | $\ln(ISDR_{max})$ = -4.280+0.94089ln ($PGA$) | 0.730 | 0.1958 |
| Earthquake sequence$\delta$ = 0.8 | $\ln(ISDR_{max})$ = -4.164+0.96491ln ($PGA$) | 0.735 | 0.2007 |

were used to generate foreshock-mainshock-aftershock sequence-type ground motions.

To obtain the most reasonable PSDM for the structural calculation, it is essential to select representative ground motion IMs and EDPs. At present, the commonly used IMs include the peak ground acceleration (PGA) and spectral acceleration ($S_a$) (Nielson 2005). By referencing the previous studies (e.g., Choi *et al.* 2004, Nielson. 2005, Li *et al.* 2018), the simple and intuitive PGA is adopted as the ground motion IM to perform a seismic fragility analysis of PEDSW-2 herein. Currently, the ISDR is often selected as an important index for damage assessment in the fragility analysis of RC building structures (Li *et al.* 2018). Compared to the roof displacement and base shear of a structure, the ISDR can not only directly reflect the displacement variation between the floors of a shear wall structure but can also indirectly represent the local damage of the shear wall components. Therefore, the ISDR was selected in this study as the EDP in the fragility analysis of a high-rise PEDSW (PEDSW-2).

Fig. 14(a) shows samples of the seismic response analysis results of PEDSW-2 under a single mainshock and under three different earthquake sequences ($\delta$=0.4, 0.6, 0.8). In the figure, the horizontal axis is the logarithmic PGA (ln ($PGA$)) and the vertical axis is the logarithmic value of the maximum ISDR (ln ($ISDR_{max}$)). The logarithmic linear regression analyses on the samples of the seismic response analysis results were conducted. Figs. 14(b), (c) and (d) compares the results of the regression analysis of the dynamic responses under a single mainshock and under different earthquake sequences ($\delta$=0.4, 0.6, 0.8). Table 4 lists the parameters of the PSDM under different cases. It can be seen that the $ISDR_{max}$ and IM of PEDSW-2 comply well with a logarithmic linear relationship under different ground motion conditions, and as the aftershock intensity increases, the influence of the earthquake sequence on the EDP also gradually increases.

### *4.2 Results and analysis*

Assuming the structural seismic demands follow a logarithmic linear distribution at different IM levels, based on the PSDA analysis results, the seismic fragility function

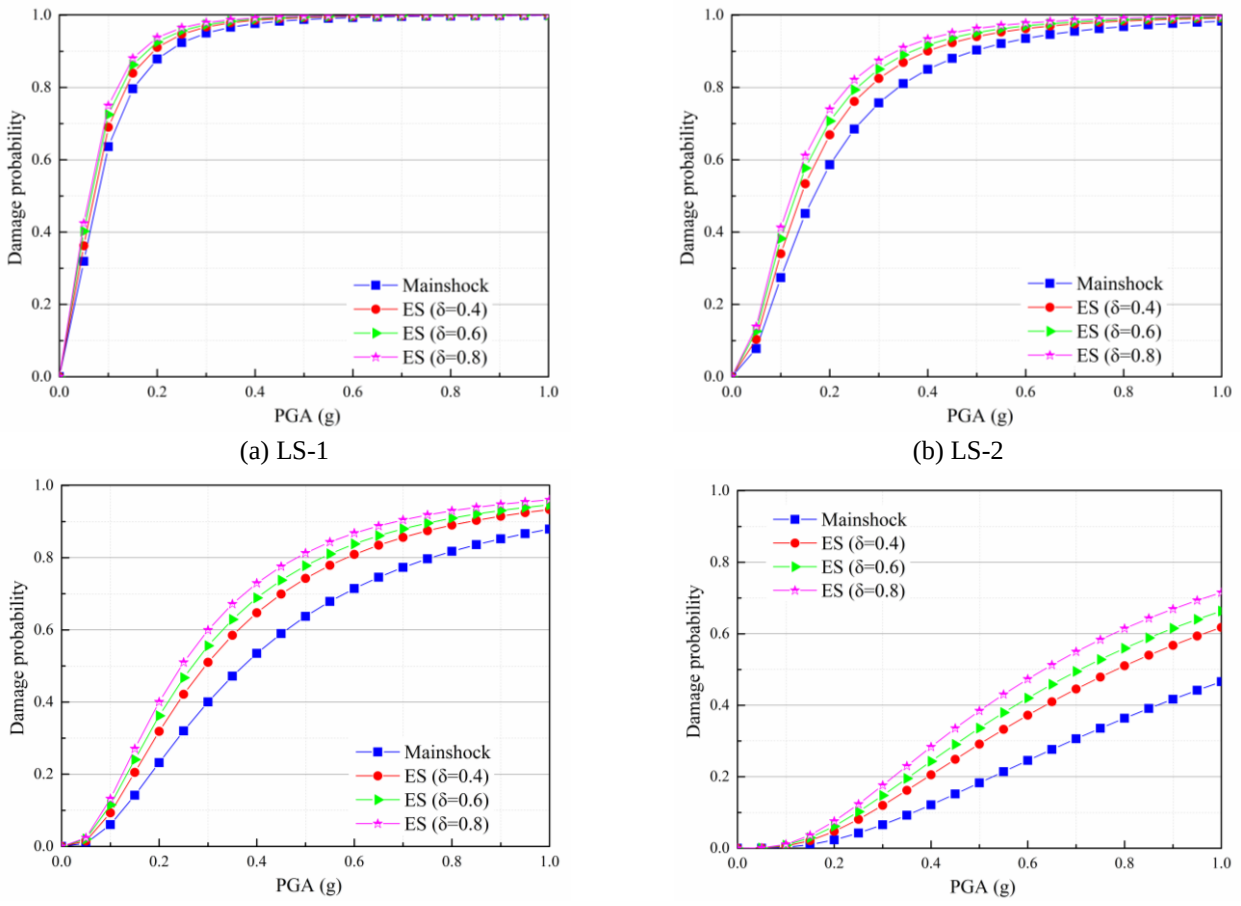


(a) LS-1 (b) LS-2

(c) LS-3 (d) LS-4

Fig. 15 Comparison of seismic fragility curves of PEDSW-2 under mainshock and various earthquake sequences

Table 5 Classification of damage limit states

| Damage limit States | LS-1 | LS-2 | LS-3 | LS-4 |
|---|---|---|---|---|
| $ISDR_{max}$ | 0.001 | 0.002 | 0.005 | 0.01 |

is written by

$$P(D \geq C \mid IM) = \Phi\left[\frac{\ln(\mu_D) - \ln(\mu_C)}{\sqrt{\sigma_{D|IM}^2 + \sigma_C^2}}\right] \tag{3}$$

where $D$ and $C$ are the seismic demand and structural capacity, respectively; $\mu_D$and $\mu_C$ are the median values of $D$ and $C$; and $\sigma_{D|IM}$ and $\sigma_C$ are the corresponding standard deviations, where $\sigma_C$ takes a value of 0.4 (Li *et al.* 2018).

The seismic fragility characterizes the conditional probability that a structure exceeds a certain limit state of failure underground motions with different intensities. Therefore, the definition of the limit state is an important part of the structural seismic capacity analysis. Based on the selected structural damage index ($ISDR_{max}$), four limit states are defined for PEDSW-2, i.e., slight damage (LS-1), moderate damage (LS-2), severe damage (LS-3), and collapse (LS-4). The $ISDR_{max}$ values corresponding to the different damage limit states are shown in Table 5.

Fig. 15 shows fragility curves of the high-rise PEDSW (PEDSW-2) in different damage limit states under a single mainshock and different earthquake sequences ($\delta$=0.4, 0.6, 0.8). Compared with that under a single mainshock, the structural fragility significantly increased under an earthquake sequence, and the structural failure probability increased with $\delta$. The median GPAs of the fragility of PEDSW-2 exceeding LS-1, LS-2, LS-3, and LS-4 under the earthquake sequence with $\delta$=0.4 are 0.067 g, 0.140 g, 0.294 g, and 0.783 g, respectively, amounting to decreases of 9.46%, 15.66%, 20.75%, and 27.16%, respectively, compared to that under a single mainshock (0.074 g, 0.166 g, 0.371 g, 1.075 g). The median PGAs of the fragility of the PEDSW exceeding LS-1, LS-2, LS-3, and LS-4 under the earthquake sequence with $\delta$=0.6 are 0.061 g, 0.128 g, 0.267 g, and 0.708 g, showing decreases of 17.57%, 22.89%, 28.03%, and 34.14%, respectively, compared to that under a single mainshock, and the median PGAs with $\delta$=0.8 are 0.058 g, 0.119 g, 0.245 g, and 0.633 g, respectively, representing decreases of 21.62%, 28.31%, 33.96%, and 41.11%, respectively). Compared with the case of a single mainshock, the same damage limit state of the PEDSW would be triggered under the foreshock-mainshock-aftershock sequence with a smaller PGA vale, and with the increase of the scaling factor $\delta$, the effect of the earthquake sequence on the fragility of PEDSW-2 increased significantly.

It is also observed that the influence of earthquake

sequence on the seismic fragility under slight damage state is minor, since the fragility curves for different cases are quite close to each other (as shown in Fig. 15(a)).However, with the increase of damage state, the impact of earthquake sequence on the fragility curves becomes more evident (as shown in Figs. 15(a), 15(b) and 15(c)). Taking PGA=0.2 g as an example, the probability of slight damage (LS-1) under a single mainshock is 87.86%, while that under the earthquake sequences ($\delta$=0.4, 0.6, 0.8) are 91.08%, 92.56%, and 93.79%, respectively, representing increases of 3.67%, 5.35%, and 6.75% compared with the case of a single mainshock. The exceedance probability of structural collapse (LS-4) under a single mainshock is 4.24%, while that under the earthquake sequences ($\delta$=0.4, 0.6, 0.8) are4.72%, 6.16%, and 7.55%, respectively, representing increase of 11.40%, 45.33% and 78.20% compared to the case of a single mainshock. In summary, an earthquake sequence can considerably increase the damage probability of the PEDSW structure, and the consideration of only a single mainshock would lead to underestimated seismic fragilities and unsafe structural design schemes, especially for moderate, severe and collapse damage states.

## 5. Conclusions

In this paper, the seismic performance of PEDSW and SIPSW were comparatively analyzed using numerical simulation approach.

Based on the probabilistic seismic demand analysis (PSDA), the fragility curves of the PESDW structure under a single mainshock and under different earthquake sequences were generated, and the following key conclusions are drawn:

- The continuous round-hole mild steel dampers exhibited a stable force-displacement hysteresis curve and excellent energy dissipation capacity under cyclic loading. The application of the dampers as dry connectors to assemble PCSWs can attain basically equivalent load-carrying capacity and lateral stiffness as those of CIPSWs. Therefore, it is feasible to use mild steel dampers as connectors for the PCSWs.
- A comparative analysis of the nonlinear seismic response of the high-rise PEDSW and the CIPSW demonstrated that the PEDSW can effectively decrease the structural seismic response and the concrete damage of wall panels. Compared to that of the cast-in-place wall, the reduction percentages of the maximum roof displacement and ISDR of the PEDSW could reach 45.15% and 44.53%, respectively. The use of mild steel dampers as connectors can effectively help the structural system to dissipate seismic energy and improve the seismic resistance capability of PCSW structures.
- Compared with those of a single mainshock, the maximum roof displacement and ISDR of the PESDW structure under an earthquake sequence increased significantly with the increasing scaling factor $\delta$. When $\delta$=0.8, the increase ratio of the maximum roof displacement and ISDR of the exemplar structure can reach 84.35% and 81.83%, respectively. With the increase of the scaling factor $\delta$, the increase ratio of the seismic response became more significant, and the damage to the wall panel concrete was also more serious.
- The fragility of the PEDSW under an earthquake sequence was significantly higher than that under a single mainshock. Although the impact of earthquake sequence on the seismic fragility of PEDSW under the slight damage state is relatively minor, the influences of foreshocks and aftershocks on the fragility curves becomes very significant for the higher limit states. Thereby, special emphasis should be placed on the adverse effect of earthquake sequence on the seismic performance of PCSW structures, especially for the collapse damage state.

It should be noted that the proposed PEDSW is a new system, which is not mature and not applied in engineering practice yet. This paper is a preliminary numerical investigation on the seismic performance of the PEDSW under earthquake sequences. The feasibility and effectiveness of the proposed PEDSW are validated by comparing the seismic performance with that of the traditional CIPSW. In the future studies, the proposed PEDSW can be further improved by connecting shear walls and the base with pre-stressed reinforcing steels and allowing rocking motions at the bottom of shear walls, which can more effectively exert the energy dissipation capacity of mild steel dampers. Moreover, the cyclic loading tests and shaking table tests should be carried out to further explore the earthquake resistant behavior of the PEDSWs and provide valuable suggestions for the relevant design specifications.

## Acknowledgments

The authors would like to thank the financial supports from the National Key R&D Program of China (2018YFD1100404, 2016YFC0701108) and the State Key Program of National Natural Science Foundation of China (51738007) for carrying out this research. The supports from the Natural Science Foundation of Liaoning Province (20180550949) and the Program of Guangdong Key Laboratory of Earthquake Engineering and Application Technology (2017B030314068) are also gratefully acknowledged.

## References

Allahvirdizadeh, R. and Mohammadi, M.A. (2016), "Upgrading equivalent static method of seismic designs to performance-based procedure", *Earthq. Struct.*, **10**(4), 849-865. https://doi.org/10.12989/eas.2016.10.4.849.

Amadio, C., Fragiacomo, M. and Rajgelj, S. (2003), "The effects of repeated earthquake ground motions on the non-linear response of SDOF systems", *Earthq. Eng. Struct. Dyn.*, **32**(2), 291-308. https://doi.org/10.1002/eqe.225.

Becker, J.M., Llorente, C. and Mueller, P. (1980), "Seismic response of precast concrete walls", *Earthq. Eng. Struct. Dyn.*, **8**(6), 545-564. https://doi.org/10.1002/eqe.4290080605.

Beilic, D., Casotto, C, Nascimbene, R., Cicola, D. and Rodrigues, D. (2017), "Seismic fragility curves of single storey RC precast

structures by comparing different Italian codes", *Earthq. Struct.*, **12**(3), 359-374. https://doi.org/10.12989/eas.2017.12.3.359.

Bljuger, F. (1976), "Determination of deformability characteristics of vertical shear joints in precast buildings", *Build. Environ.*, **11**(4), 277-282. https://doi.org/10.1016/0360-1323(76)90035-4.

Chakrabarti, S.C., Nayak, G.C. and Paul, D.K. (1988), "Shear characteristics of cast-in-place vertical joints in story-high precast wall assembly", *ACI Struct. J.*, **85**(1), 30-45. https://doi.org/10.14359/2965.

Choi, E., DesRoches, R. and Nielson, B. (2004). "Seismic fragility of typical bridges in moderate seismic zones", *Eng. Struct.*, **26**(2), 187-199. https://doi.org/10.1016/j.engstruct. 2003.09.006.

Cornell, C.A., Jalayer, F., Hamburger, R.O. and Foutch, D.A. (2002), "Probabilistic basis for 2000 SAC federal emergency management agency steel moment frame guidelines", *J. Struct. Eng.*, **128**(4), 526-533. https://doi.org/10.1061/(ASCE)0733-9445(2002)128:4(526).

Crisafulli, F.J. and Restrepo, J.I. (2003), "Ductile steel connections for seismic resistant precast buildings", *J. Earthq. Eng.*, **7**(4), 541-553. https://doi.org/10.1080/13632460309350463.

Fajfar, P. (2000), "A nonlinear analysis method for performance-based seismic design", *Earthq. Spectra*, **16**(3), 573-592. https://doi.org/10.1193/1.1586128.

Fib-bulletin 43(1999), Structural Connections for Precast Concrete Buildings.

Fib-bulletin 63(2012), Design of Precast Concrete Structures Against Accidental Actions.

GB50011-2010 (2010), Code for Seismic Design of Buildings, China Architecture and Building Press, Beijing, China.

Guo, W., Zhai, Z.P., Cui, Y., Yu, Z.W. and Wu, X.L. (2019), "Seismic performance assessment of low-rise precast wall panel structure with bolt connections", *Eng. Struct.*, **181**, 562-578. https://doi.org/10.1016/j.engstruct.2018.12.060.

Han, L.B., Cheng, J., An, Y.R., Fang, L.H., Jiang, C.S., Chen, B., Wu, Z.L., Liu, J., Xu, X.W., Liu, R.F., Yao, Z.X., Wang, C.Z. and Wang, Y.S. (2018), "Preliminary report on the 8 August 2017 Ms 7.0 Jiuzhaigou, Sichuan, China, earthquake", *Seismol. Res. Lett.*, **89**(2), 557-569. https://doi.org/10.1785/0220170158.

Hatzigeorgiou, G.D. (2010), "Behavior factors for nonlinear structures subjected to multiple near-fault earthquakes", *Comput. Struct.*, **88**(5), 309-321. https://doi.org/10.1016/j.compstruc.2009. 11.006.

Hatzigeorgiou, G.D. (2010), "Ductility demand spectra for multiple near- and far-fault earthquakes", *Soil Dyn. Earthq. Eng*., **30**(4), 170-183. https://doi.org/10.1016/j.soildyn.2009.10. 003.

Hatzigeorgiou, G.D. and Beskos, D.E. (2009), "Inelastic displacement ratios for SDOF structures subjected to repeated earthquakes", *Eng. Struct.*, **31**(11), 2744-2755. https://doi.org/10.1016/j.engstruct. 2009.07.002.

Herfelt, M.A., Poulsen, P.N., Hoang, L.C. and Jensen, J.F. (2016), "Numerical limit analysis of keyed shear joints in concrete structures", *Struct. Concrete*, **17**(3), 481-490. https://doi.org/10.1002/suco.201500161.

Hirose, F., Miyaoka, K., Hayashimoto, N., Yamazaki, T. and Nakamura, M. (2011), "Outline of the 2011 off the Pacific coast of Tohoku Earthquake (Mw 9.0)-Seismicity: foreshocks, mainshock, aftershocks, and induced activity", *Earth Plan. Space*, **63**(7), 513-518. https://doi.org/10.5047/eps. 2011.05.019.

Huang, R.Q. and Li, W.L. (2009), "Development and distribution of geohazards triggered by the 5.12 Wenchuan Earthquake in China", *Sci. China Ser. E: Technol. Sci.*, **52**(4), 810-819. https://doi.org/10.1007/s11431-009-0117-1.

Hutchinson, R.L., Rizkalla, S.H., Lau, M. and Heuvel, S. (1991), "Horizontal post-tensioned connections for precast concrete load bearing shear wall panels", *PCI J.*, **36**(6), 64-76. https://doi.org/10.15554/pcij.11011991.64.76.

Jiang, H.K., Li, Y.L., Qu, Y.J., Hua, A.J., Zheng, J.C., Dai, L. and Hou, H.F. (2006), "Spatial distribution features of sequence types of moderate and strong earthquake in Chinese mainland", *Acta Seismologica Sinica*, **19**(4), 417-427. https://doi.org/10.1007/s11589-004-0417-5.

Kurama, Y.C. (2005), "Seismic design of partially post-tensioned precast concrete walls", *PCI J.*, **50**(4), 100-125. https://doi.org/10.15554/pcij.07012005.100.125.

Kwon, O.S. and Elnashai, A. (2006), "The effect of material and ground motion uncertainty on the seismic vulnerability curves of RC structure", *Eng. Struct.*, **28**(2), 289-303. https://doi.org/10.1016/j.engstruct.2005.07.010.

Li, C., Hao, H., Li, H.N. and Bi, K.M. (2015), "Theoretical modeling and numerical simulation of seismic motions at seafloor", *Soil Dyn. Earthq. Eng.*, **77**, 220-225. https://doi.org/10.1016/j.soildyn.2015.05.016.

Li, C., Hao, H., Li, H.N. and Bi, K.M. (2016), "Seismic fragility analysis of reinforced concrete bridges with chloride induced corrosion subjected to spatially varying ground motions", *Int. J. Struct. Stab. Dyn.*, **16**(05), 1550010. https://doi.org/10.1142/S0219455415500108.

Li, C., Hao, H., Li, H.N., Bi, K.M. and Chen B.K. (2017), "Modeling and simulation of spatially correlated ground motions at multiple onshore and offshore sites", *J. Earthq. Eng.*, **21**(3), 359-383. https://doi.org/10.1080/13632469.2016.1172375.

Li, C., Li, H.N., Hao, H., Bi, K.M. and Chen, B.K. (2018), "Seismic fragility analyses of sea-crossing cable-stayed bridges subjected to multi-support ground motions on offshore sites", *Eng. Struct.*, **165**, 441-456. https://doi.org/10.1016/j.engstruct. 2018.03.066.

Li, L.X., Li, H.N. and Li, C. (2018), "Seismic fragility assessment of self-centering RC frame structures considering maximum and residual deformations", *Struct. Eng. Mech.*, **68**(6), 677-689. https://doi.org/10.12989/sem.2018.68.6.677.

Li, Q. and Ellingwood, B.R. (2007), "Performance evaluation and damage assessment of steel frame buildings under mainshock-aftershock earthquake sequences", *Earthq. Eng. Struct. Dyn.*, **36**(3), 405-427. https://doi.org/10.1002/eqe.667.

Li, R.H., Li, H.N. and Li, C. (2018), "Seismic performance assessment of RC frame structures subjected to far-field and near-field ground motions considering strain rate effect", *Int. J. Struct. Stab. Dyn.*, **18**(10), 1850127. https://doi.org/10.1142/S0219455418501274.

Li, S., Tian, J. and Liu, Y. (2017), "Performance-based seismic design of eccentrically braced steel frames using target drift and failure mode", *Earthq. Struct.*, **13**(5), 443-454. http://dx.doi.org/10.12989/eas.2017.13.5.443.

Li, Y., Song, R. and van de Lindt John, W. (2014), "Collapse fragility of steel structures subjected to earthquake mainshock-aftershock sequences", *J. Struct. Eng.*, **140**(12), 04014095. https://doi.org/10.1061/(ASCE)ST.1943541X.0001019.

Lim, W.Y., Kang, H.K. and Hong, S.G. (2016), "Cyclic lateral testing of precast concrete T-walls in fast low-rise construction", *ACI Struct. J.*, **113**(1), 179-89. https://doi.org/10.14359/51688200.

Liolios, A., Elenas, A., Liolios, A., Radev, S., Georgiev, K. and Georgiev, I. (2014), "Tall RC buildings environmentally degradated and strengthened by cables under multiple earthquakes: a numerical approach", *International Conference Numerical Methods Applications*, **8962**, 187-195. https://doi.org/10.1007/978-3-319-15585-2_21.

Mackie, K. and Stojadinović, B. (2005), "Fragility basis for California highway overpass bridge seismic decision making", PEER Report No. 2005/02, Pacific Earthquake Engineering Research Center, University of California, Berkeley, U.S.A.

Magliulo, G., Ercolino, M., Petrone, C., Coppola, O. and

Manfredi, G. (2014), "The Emilia earthquake: seismic performance of precast reinforced concrete buildings", *Earthq. Spectra*, **30**(2), 891-912. https://doi.org/10.1193/091012EQS285M.

Mahin, S.A. (1980), "Effects of duration and aftershocks on inelastic design earthquakes", *Proceedings of the Seventh World Conference on Earthquake Engineering*, **5**, 677-679.

Naderpour, H. and Vakili, K. (2019), "Safety assessment of dual shear wall-frame structures subject to mainshock-aftershock sequence in terms of fragility and vulnerability curves", *Earthq. Struct.*, **16**(4), 425-436. https://doi.org/10.12989/eas.2019.16.4.425.

Nastri, E., Vergato, M. and Latour, M. (2017), "Performance evaluation of a seismic retrofitted RC precast industrial building", *Earthq. Struct.*, **12**(1), 13-21. https://doi.org/10.12989/eas.2017.12.1.013.

Nazari, N., van de Lindt, J.W. and Li, Y. (2015), "Effect of mainshock-aftershock sequences on woodframe building damage fragilities", *J. Perform. Constr. Facil.*, **29**(1), 04014036. https://doi.org/10.1061/(ASCE)CF.19435509.0000512.

Nielson, B.G. (2005), "Analytical fragility curves for highway bridges in moderate seismic zones", Ph.D. Dissertation, Georgia Institute of Technology, Georgia, U.S.A.

Ozden, S. and Ertas, O. (2007), "Behavior of unbonded, post-tensioned, precast concrete connections with different percentages of mild steel reinforcement", *PCI J.*, **52**(2), 32-44. https://doi.org/10.15554/pcij.03012007.32.44.

Pall, A.S., Marsh, C. and Fazio, P. (1982), "Friction joints for seismic control of large panel structures", *PCI J.*, **25**(6), 38-61. https://doi.org/10.15554/pcij.11011980.38.61.

Pantelides, C.P, Volnyy, V.A., Gergely, J. and Reaveley, L.D. (2003), "Seismic retrofit of precast concrete panel connections with carbon fiber reinforced polymer composites", *PCI J.*, **48**(1), 92-104. https://doi.org/10.15554/pcij.01012003.92.104.

Park, R. (1995), "A perspective on the seismic design of precast concrete structures in New Zealand", *PCI J.*, **40**(3), 40-60. https://doi.org/10.15554/pcij.05011995.40.60.

Park, R. (2002), "Seismic design and construction of precast concrete buildings in New Zealand", *PCI J.*, **47**(5), 60-75. https://doi.org/10.15554/pcij.09012002.60.75.

Park, R. (2003), "The fib state-of-the-art report on the seismic design of precast concrete building structures", *Pacific Conference on Earthquake Engineering*.

Pekau, O.A. and Hum, D. (1991), "Seismic response of friction jointed precast panel shear walls", *PCI J.*, **36**(2), 56-71. https://doi.org/10.15554/pcij.03011991.56.71.

Perez, F.J., Sause, R. and Pessiki, S. (2007), "Analytical and experimental lateral load behavior of unbonded posttensioned precast concrete walls", *J. Struct. Eng.*, **133**(11), 1531-1540. https://doi.org/10.1061/(asce)07339445(2007)133:11(1531).

Pessiki, S. and Perez, F.J. (2004), "Seismic design of unbonded post-tensioned precast concrete walls with vertical joint connectors", *PCI J.*, **49**(1), 58-79. https://doi.org/10.15554/pcij.01012004.58.79.

Reaveley, L.D. and Pantelides, C.P. (2002), "Behavior of welded plate connections in precast concrete panels under simulated seismic loads", *PCI J.*, **47**(4), 122-133. https://doi.org/10.15554/pcij.07012002.122.133.

Rizkalla, S.H., Serrette, R.L., Heuvel, J.S. and Attiogbe, E. (1989), "Multiple shear key connections for precast shear wall panels", *PCI J.*, **34**(2), 104-120. https://doi.org /10.15554/pcij.03011989.104.120.

Sakata, H., Kuboyama, H., Sugiyama, T. and Ikezawa, M. (2005), "Experimental study on beam-column joint of damage controlled precast-prestressed concrete frame with P/C mild-press-joint", *J. Struct. Constr. Eng.*, **2005**(588), 141-148. https://doi.org/10.3130/aijs.70.141-1.

Shome, N. and Cornell, C.A. (1999), "Probabilistic seismic demand analysis of nonlinear structures", Reliability of Marine Structures Report No. RMS-35, Stanford University, California.

Shrestha, B., Li, C., Hao, H. and Li, H.N. (2017), "Performance-based seismic assessment of superelastic shape memory alloy-reinforced bridge piers considering residual deformations", *J. Earthq. Eng.*, **21**(7), 1050-1069. https://doi.org/10.1080/13632469. 2016.1190798.

Simulia, D. (2011), Abaqus 6.11 Analysis User's Manual.

Soudki, K.A., Rizkalla, S.H. and Leblanc, B. (1995), "Horizontal connections for precast concrete shear walls subjected to cyclic deformations part.1. Mild-steel connections", *PCI J.*, **40**(4), 78-96. https://doi.org/10.15554/pcij.07011995.78.96.

Soudki, K.A., West, J.S., Rizkalla, S.H. and Blackett, B. (1996), "Horizontal connections for precast concrete shear wall panels under cyclic shear loading", *PCI J.*, **41**(3), 64-80. https://doi.org/10.15554/pcij.05011996.64.80.

Sritharan, S., Aaleti, S., Henry, R.S., Liu, K.Y. and Tsai, K.C. (2015), "Precast concrete wall with end columns (PreWEC) for earthquake resistant design", *Earthq. Eng. Struct. Dyn.*, **44**(12), 2075-2092. https://doi.org/10.1002/eqe.2576.

Sugata, M. and Nakatsuka, T. (2005), "Estimation for load-deflection characteristics of precast prestressed flexural member with unbonded tendons and mild steel using a macro model", *J. Struct. Constr. Eng.*, **70**(590), 103-110. https://doi.org/10.3130/aijs.70.103-2.

Wen, W., Zhai, C., Ji, D., Li, S. and Xie L. (2017), "Framework for the vulnerability assessment of structure under mainshock-aftershock sequences", *Soil Dyn. Earthq. Eng.*, **101**, 41-52. https://doi.org/10.1016/j.soildyn.2017.07.002.

Xu, G., Wang, Z., Wu, B. and Bursi, O.S. (2017), "Seismic performance of precast shear wall with sleeves connection based on experimental and numerical studies", *Eng. Struct.*, **150**, 346-58. https://doi.org/10.1016/j.engstruct.2017.06.026.

Zhang, C.Y., Li, H.N., Gao, W.H. and Li, C. (2019), "Experimental and analytical investigations on new viscoelastic damped joints (VDJs) for seismic mitigation of structures with precast shear walls", *Struct. Control Hlth. Monit.*, e2485, 1-25. https://doi.org/10.1002/stc.2485.

Zhang, H., Li, H.N., Li, C. and Cao, G.W. (2018), "Experimental and numerical investigations on seismic responses of reinforced concrete structures considering strain rate effect", *Constr. Build. Mater.*, **173**, 672-686. https://doi.org/10.1016/j.conbuildmat.2018.04.085.

Zhu, Z.F. and Guo, Z.X. (2019), "Seismic performance of the spatial model of precast concrete shear wall structure using grouted lap splice connection andcast-in-situ concrete", *Struct. Concrete*, 1-12. https://doi.org/10.1002/suco.201800252.

*CC*